Impact of Feedstock Properties on the Deactivation of a Vacuum Gas oil Hydrocracking Catalyst

July C Vivas-Báez, Gerhard Pirngruber, Alberto Servia, Anne-Claire Dubreuil, David J Pérez-Martínez

IMPACT OF FEEDSTOCK PROPERTIES ON THE DEACTIVATION OF A VACUUM GASOIL HYDROCRACKING CATALYST

July C. VIVAS-BÁEZ[a,b], Gerhard PIRNGRUBER[a], Alberto SERVIA[a], Anne-Claire DUBREUIL[a], David J. PÉREZ-MARTÍNEZ[b]

a IFP Energies nouvelles, Rond-point de l'échangeur de Solaize, France, 69360.
b Centro de innovación y tecnología ICP, ECOPETROL S.A., Km 7 vía Piedecuesta, Piedecuesta, Colombia, 681011.
Corresponding Author: Gerhard PIRNGRUBER (mailto:gerhard.pirngruber@ifpen.fr)

Keywords: deactivation, hydrocracking, coking, nitrogen poisoning, vacuum gasoil.

ABSTRACT

The aim of this study was to understand the impact of vacuum gas oil (VGO) properties on the deactivation rate of a hydrocracking catalyst (a nickel-molybdenum sulfide dispersed on a carrier containing USY zeolite). For that purpose, two hydrotreated feeds of different density, organic nitrogen (~120-150 ppmw) and aromatic content, were hydrocracked under operating conditions that favor catalyst deactivation, i.e., high temperature (T=418°C) and high space velocity (LHSV=3 h^{-1}). The catalyst performance was followed by measuring the VGO conversion (370°C$^+$ petroleum cut) and determining the apparent kinetic constants for the main hydrocracking reactions (cracking, hydrodenitrogenation, hydrodesulfurization and aromatics hydrogenation). The experiments were stopped after different times on stream (either 6 or 30 days) in order to assess the evolution of the catalyst as a function of time. The spent catalysts, obtained from three different reactor locations, were characterized by elemental and textural analysis and by thermogravimetry to investigate the quantity and nature of the coke formed. Catalytic tests with different model compounds (toluene, n-heptane) were carried out to determine the residual activity of the hydrogenating and acid catalyst functions. It was found that, at the evaluated conditions, both organic nitrogen and aromatics, nature and content of the feedstock, have a determinant role on

the deactivation rate. The organic nitrogen determines the ratio between available metal and acid sites. The aromatics generate coke precursors on the available acid sites. Both factors play a coupled role that promotes coke deposition on the catalyst surface, which leads to an increase in the deactivation rate on top of the end boiling point of the feed.

1 INTRODUCTION

Catalyst deactivation is a physical and/or chemical process that decreases the activity of a given catalyst [1]. The deactivation is a problem of great concern in the practice of industrial catalytic processes. Costs for catalyst replacement and process shutdown total billions of dollars per year [2]. Deactivation depends on feedstock, operating conditions and catalyst properties [3]. Concerning the feedstocks, it is known that in the hydrocracking of vacuum gasoils (VGO), the formation of coke and quasi-irreversible poisoning by heavy nitrogen molecules are the primary reasons for catalyst deactivation [4,5]. The contribution of metals to deactivation becomes evident with deasphalted oil and increases as the feed becomes heavier, such as with atmospheric and vacuum residues [6].

Carbonaceous deposits (“coke”) on catalysts are gradually formed during the hydrocarbon conversion reactions. Deactivation by coke is due to physical blocking of active sites or because large amounts of coke can lead to pore blocking and prevent reactant molecules from reaching the active sites inside the pores [1]. Coke formation depends on the type of processed feed. For example, aromatic feedstocks form more coke than aliphatic ones under similar processing conditions because polyaromatic structures are more easily formed from aromatics [7]. Coking is more pronounced with condensed ring systems (e.g., naphthalene, anthracene) than with the corresponding linked systems (biphenyl, terphenyl) [8,9]. Heterocycles produce more coke than hydrocarbon analogs [10]. For alkyl-substituted aromatics, coke deposition increases with the length of the side chains rather than with the number of alkyl substitutions [9]. In the case of heavy

oils and residues, precipitation of asphaltenes from the feed is another important source of coke formation [11]. Asphaltenes are stabilized by the presence of resins. Therefore, if resins are eliminated at a faster rate during hydroprocessing of asphaltenes, precipitation of the latter occurs on the surface of the catalyst, leading to the possibility of greater coke formation [12]. Several studies [13–17] on catalyst deactivation by coke deposits during the hydroprocessing of AR and VR without considering the metals concluded that the coke formed during the early stages of the operation deposited on the support rather than on active phase. However, while coke reaches pseudo-steady-state equilibrium after an initial rapid buildup [18,19], the deposition of metals continuously increases with time-on-stream [20,21]. To various degrees, the deactivation by coke and metals occurs simultaneously.

Two different mechanisms have been proposed for coke formation on the metal and the acid sites for bifunctional catalysts. On metal sites, it is presumed that coke results from successive dehydrogenations leading to atomic carbon or partially hydrogenated intermediates that combine to form graphitic coke [22,23]. On acid sites, it is accepted that coke results from polymerization of dehydrogenated intermediates generated on the metal sites [24].

Concerning spent catalysts from VGO hydroprocessing, Sahoo et al. [25] characterized two samples after a dichloromethane extraction. The soluble part was termed as “soft coke,” and its structure was similar to those of the VGO heavy components. The insoluble part, named as “hard coke”, was more aromatic. Coke on catalysts deactivated during the hydroprocessing of atmospheric (ARs) and vacuum residues (VRs) is even “harder”. Amemiya et al. [26] took catalyst samples from a VGO hydroprocessing unit after 12 months on stream. These samples were extracted from different locations in the axial direction of a single fixed bed. The amount and the graphitic nature of the coke increased toward the end of the bed. Koizumi et al. [27] also found an amorphous coke structure at the inlet and a graphitic structure at the catalyst bed outlet.

75 Nitrogen compounds play an important role in the deactivation. The type of N-compounds and the
76 total amount of nitrogen vary from feed to feed [28]. The five and six-membered N-rings, classified
77 as non-basic “neutral” and basic N-compounds, respectively, are predominant structures [29]. The
78 less basic or neutral nitrogen derivatives are readily decomposed into ammonia [30], which acts
79 as an inhibitor of the cracking reaction. The more basic compounds are cataloged as poisons as
80 they are strongly adsorbed on the acid sites of the catalyst [31].

81 N-compounds hinder the adsorption of other reactants and slow down the hydrogen activation
82 process [32]. The availability of active surface hydrogen [33] for the other hydroprocessing
83 reactions and the coke formation is thus limited. Therefore, at least part of the coke is formed due
84 to the catalyst poisoning by N-compounds. Studies on model compounds and real feeds indicate
85 that less than 50 ppm of organic nitrogen in the feed can poison catalytic sites [4,34]. The important
86 contribution of N-compounds to catalyst deactivation during the hydroprocessing of a VGO was
87 also confirmed by Massoth et al. [35]. However, due to the slow desorption of N-compounds from
88 the acid sites [5], it is sometimes difficult to distinguish strong inhibition [36,37] (i.e. the direct
89 impact on conversion via adsorption on the active sites) from deactivation (i.e. the indirect impact
90 via favoring coke formation).

91 In our recent work [38], an accelerated deactivation procedure for hydrocracking catalysts was
92 developed using real feeds (VGO) at conditions close to typical process conditions. The aged
93 catalysts from this protocol showed comparable properties to some industrial spent catalysts.
94 Through this experimental procedure, it was found that the organic nitrogen content of the
95 feedstock is crucial since it determines the ratio between the available metal and acid sites. In
96 turn, this ratio determines the coking reactions that take place and, therefore, the type of coke
97 produced. The nature of nitrogen compounds and of aromatic coke precursors differs depending
98 on the geographical origin of the crude and the VGO type (straight-run VGO, Coker Gas Oil, Cycle
99 Oil, etc.) [39–41]. However, studies evaluating the effect on the deactivation of these compounds

with industrial feeds are very rare in the case of VGO. This work, therefore, aims to evaluate the effect of the feedstock properties on deactivation. For this purpose, the catalyst was submitted to the mentioned protocol using two different VGO's. The reactivity evolution of the main hydrocracking reactions and the deactivation phenomena by coke and nitrogen compounds were studied in a coupled way.

2 EXPERIMENTAL SECTION

2.1 Feedstocks

Two different feedstocks were used to evaluate the impact of feedstock properties on catalyst deactivation. Feedstock A consisted of a hydrotreated straight-run vacuum gas oil (VGO-HDT); the feedstock B was a hydrotreated blend of 71% vacuum gasoil, 16% coker gasoil and 13% light cycle oil on a weight basis. The main properties of these feeds are shown in Table 1. Both feedstocks have a quite different boiling range, feed A being heavier than feed B. The distillation yields for each one are presented in Figure 1. Dimethyl disulfide and aniline were added to the hydrotreated feeds to generate the hydrogen sulfide and ammonia partial pressures representative of the mother feed containing sulfur and nitrogen contents of 1,18 wt% and 0,25 wt%, respectively.

Table 1. Feedstocks properties.

Properties		**Feed A**	**Feed B**
Density @ 15°C	g/cm^3	0.8984	0.8679
Refraction Index @ 70° C		1.4751	1.4791
Sulfur content	wt%	0.068	0.016
Nitrogen content	ppmw	149	120
Aromatics content	wt%	~37	~42
Yield of 370°C+ fraction	wt%	92	64
Initial boiling point (IBP)	°C	180	131

T50 Boiliing point	°C	461	397
Final boiling point (FBP)	°C	590	554

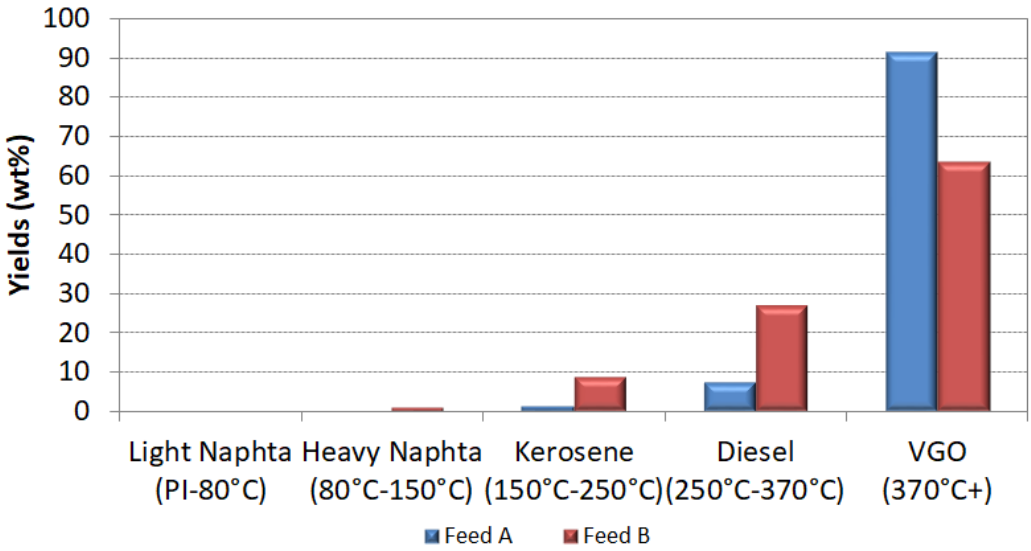

Figure 1. Cut yields for feedstocks A and B.

Considering that the main deactivation mechanisms in the deactivation of VGO hydrocracking catalysts are coking deposition and poisoning by nitrogen compounds, more detailed information about the aromatics type and the nitrogen compounds is given in Figure 2 and Figure 3, respectively. The aromatics content was ~37 wt% and ~42 wt% for feed A and feed B, respectively. Monoaromatics were the dominating family within both feeds, followed by diaromatics and triaromatics; the mass fractions of these three families were slightly higher for feed B.

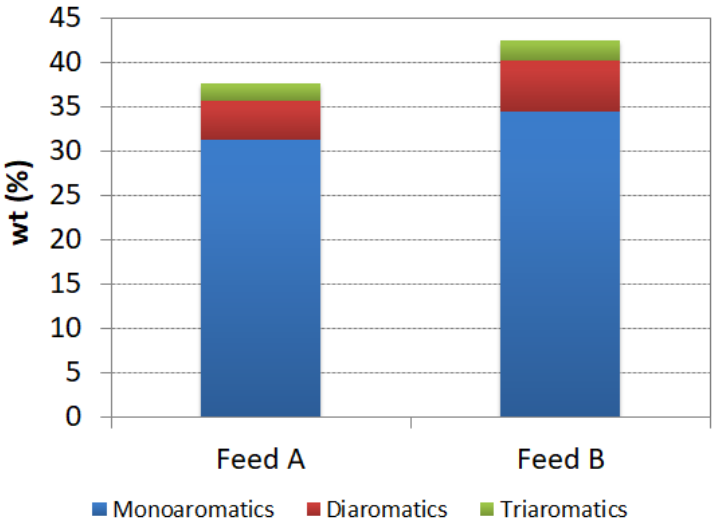

Figure 2. Aromatics type of Feeds A and B by UV spectrometry.

These feeds had a different organic nitrogen content: 149 ppmw (Basic Nitrogen - 36 ppmw) for feed A and 120 ppmw (~30 ppmw of basic nitrogen) for feed B. Such high nitrogen contents are untypical (usually hydrotreating is pushed to lower nitrogen concentration before entering the hydrocracking reactor) but were deliberately chosen to accelerate catalyst deactivation. To determine the distribution of the different nitrogen families, an analysis by FT-ICR/MS was carried out, as explained in section 2.6.1. The nitrogen families in both feedstocks are shown in Figure 3; these figures show the distribution of basic and neutral nitrogen families having the same range of double bond equivalence (DBE). The DBE plots as a function of the number of carbon atoms are provided in the supporting information (Figure S 1). The results show that feed A contained more acridine (basic nitrogen), carbazoles, benzocarbazoles and dibenzocarbazole (neutral nitrogen) than feed B. Carbazole compounds are usually considered as most refractory for the HDN reactions (they are left over at high HDN conversions) [42].

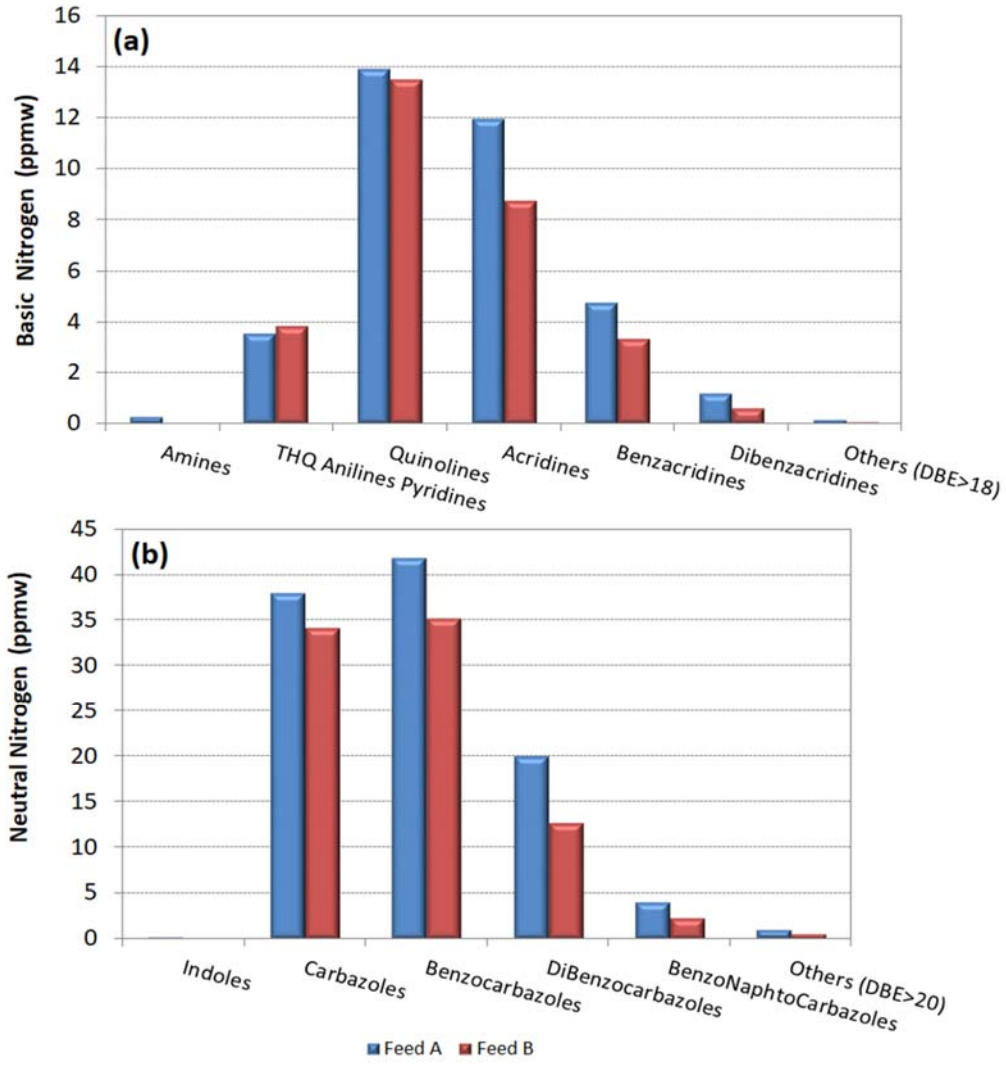

Figure 3. Concentration of representative families by DBE in (a) basic and (b) neutral nitrogen, determined by FT-ICR/MS analysis for both feeds [43].

Figure 4 presents the experimental carbon number distributions of the N-containing compounds for the two feeds. These curves are obtained from summing up the ESI (+) and ESI (−) FT-ICR/MS data. The curve for feed B shifted to a lower carbon number with respect to the curve for feed A. The carbon number for feed A is in the range of 15 to 67, whereas for feed B, the carbon number is between C10 and C60. The maximum of the carbon number distribution for feed A is around 40; meanwhile, for feed B is 33. All the above indicates nitrogen molecules of higher molecular weight for feed A associated with a higher degree of alkyl substitution.

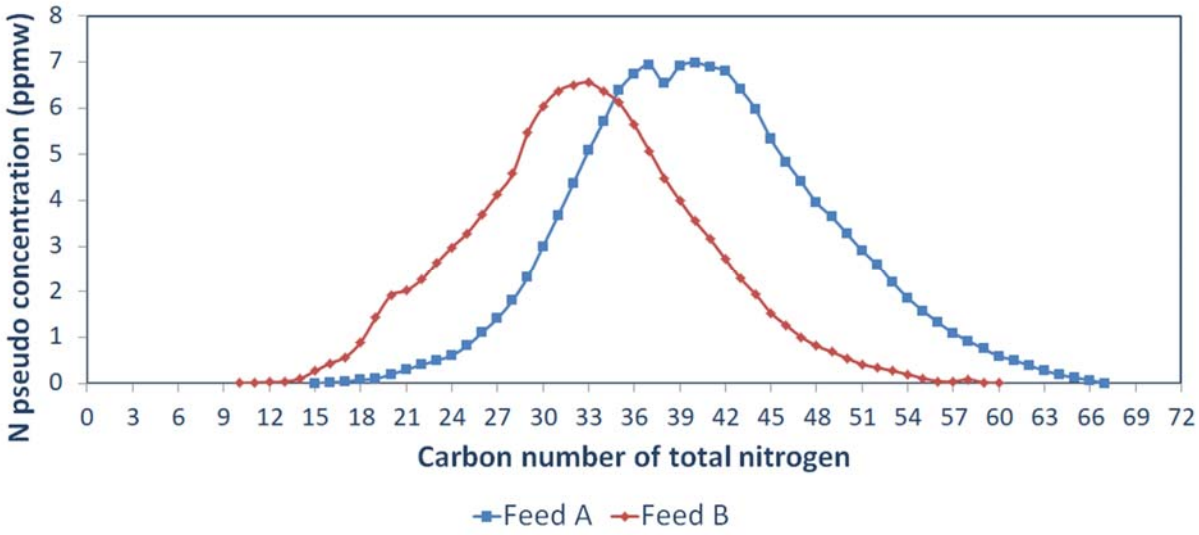

Figure 4. Carbon number distribution curves of the total nitrogen content in the feeds by FT-ICR/MS analysis [43].

2.2 Catalyst

The fresh catalyst consisted of an extrudate trilobe composed of nickel-molybdenum sulfide particles dispersed on a carrier containing USY zeolite. No additional information on catalyst properties is given for confidentiality reasons. The catalyst was diluted with silicon carbide particles of 1 mm diameter, and each reactor was loaded with 12.5 cm^3 of catalyst diluted with 37.5 cm^3 of silicon carbide.

2.3 Experimental set-up

The experiments were carried out in a fixed bed pilot unit with a co-current gas-liquid mixture flowing upwards. The detailed information has been reported elsewhere [38]. The pilot plant consisted of two isothermal reactors in series, which were used for the hydrocracking process. A liquid sampling system was placed between the two reactors. At the second reactor outlet, a high-pressure separator was installed to separate the gas and liquid phases. The gas effluent was transferred to a gas flowmeter and then analyzed by gas chromatography; the ratio H_2/HC was controlled at the gas outlet of the pilot plant. The liquid product was sent to a stripper and finally to a storage recipient. Liquid products were characterized by density, refraction index, nitrogen

and sulfur content and simulated distillation to monitor the daily performance of the catalyst. At the end of the run time (6 or 30 days), liquid samples were also analyzed to measure the aromatics, carbon and hydrogen contents.

2.4 Experimental procedure

The catalyst was activated in situ by sulfidation with an atmospheric gasoil spiked with 2% wt. (%/feed) of dimethyl disulfide (DMDS) and 2% wt. aniline (%/feed) at 350°C and 14MPa. Once sulfidation was completed, the deactivation conditions [38] were applied, i.e., 418°C, LHSV of 3 h^{-1}, H_2/HC = 1500NL/L and P = 14 MPa, with the feedstock spiked with aniline as described in section 2.1 (N_{org} = 150 ppmw, and N_{total} = 2500 ppmw). Under the conditions applied, the catalyst immediately enters a deactivation regime, which does not exhibit stabilization. However, in the analysis of the experimental results, the values of the first two days of the test were not taken into account, since at the beginning, the effects of the system stabilization and the catalyst deactivation may be overlapped. The catalyst remained at the same conditions for 6 or 30 days, depending on the test. At the end of the run, the unit was washed with atmospheric gasoil at 350°C. Subsequently, the liquid feed flow was stopped, and the catalyst was stripped and dried with hydrogen before being unloaded. Catalyst samples taken at the end of each experiment were carefully collected to separate the particles from the inlet, middle and outlet of each catalytic bed. More information about specific experimental procedures can be found elsewhere [38].

2.5 Data interpretation: kinetic laws, deactivation parameter and H2 consumption

The catalyst performance was tracked by calculating the VGO conversion (370°C$^+$ fraction) as well as the HDN, HDA and HDS conversion (Equation 1). For calculating the HDA conversion, the amount of aromatic carbon was estimated through the n-d-M method according to the standard ASTM D3238. To use this method, the molecular weight was estimated by the Lee-Kesler correlation. Yet, interpreting raw conversion data may be misleading, especially when conversion is high, because the differential reaction rate necessarily decreases when the reactant is depleted

198 at increasing conversion. For a rigorous analysis of reaction rates, a kinetic model should be
199 established, but for the complex VGO reaction network this requires a considerable amount of
200 input data [44], which was not available in our case. Therefore, for the sake of simplicity, power-
201 law models have been employed in this work. Several authors [45–47] have used this type of
202 expression to calculate these constants for similar reaction systems. A first-order [48] kinetics was
203 assumed for VGO conversion, HDN and HDA [30] (Equation 2). The first-order rate law does not
204 account for inhibition effects, but allows correcting, albeit approximately, for the impact of depleting
205 reactant concentration on the reaction rates. For HDS an apparent reaction order of 1.2 (Equation
206 3) was used; from our experience this reaction order allows accounting for the fact that S-species
207 converted at low conversions are more reactive than the refractory species left over at high
208 conversions.

$$\%\text{Conversion}=\left(\frac{mass_{x\ \text{feed}}-mass_{\text{x product}}}{mass_{\text{x feed}}}\right)*100 \qquad \text{Equation 1}$$

Where x is either the 370+ mass fraction, the nitrogen content, the sulfur content, or the aromatic carbon content.

$$k=\text{LHSV}*\ln(1-\%\text{Conversion}/100) \qquad \text{Equation 2}$$

$$k_i=\frac{\text{LHSV}}{\text{n-1}}\left(\frac{1}{\left(C_s^{\text{out}}\right)^{\text{n-1}}}-\frac{1}{\left(C_s^{\text{in}}\right)^{\text{n-1}}}\right) \qquad \text{Equation 3}$$

209 *Here n=1.2, C_s^{in}, and C_s^{out} are the feed and product concentration in percentage of sulfur.*

210 Two decay models reported in the literature based on time on stream were assumed to dissociate
211 the deactivation from the kinetic performance. An exponential decay model [46,49] with three
212 parameters (Equation 4) and an hyperbolic model [50,51] (Equation 5). The experimental data of
213 the evolution of the cracking kinetic constant with time was then fitted to each decay expression.
214

$$k_{crack}=A*\exp-(\alpha*TOS)+c \quad \text{Equation 4}$$

Where: *(A+c)* corresponds to the kinetic constant of the fresh catalyst at time=0, *c*, corresponds to the residual activity of the spent catalyst and *α* corresponds to the deactivation rate (1/time).

$$k_{crack}=A*[1+(\alpha*(m-1)*TOS)]^{-\left(\frac{1}{m-1}\right)}+d \quad \text{Equation 5}$$

Where: *(A+d)* corresponds to the kinetic constant of the fresh catalyst at time=0, *α* corresponds to the deactivation rate (1/t), *m* corresponds to the deactivation order and *d*, corresponds to the residual activity of the spent catalyst.

The hydrogen consumption was calculated from the experimental data by performing a global hydrogen balance [52] (Equation 6). It was based on the elemental analysis of liquid streams and gas chromatography. Hydrogen in gas compounds such as H_2S and light hydrocarbons (C_1 to C_6) was calculated from molar equivalents, assuming that all the light products are paraffins and all is present only in the gas product.

$$H_{cons} = H^{out}_{Liq} - H^{in}_{Liq} + H^{out}_{Light\ HC} + H^{out}_{H_2S} \quad \text{Equation 6}$$

Where H_{cons} is the hydrogen consumption, H^{out}_{Liq} is the total amount of hydrogen contained in the hydrotreated liquid product, H^{in}_{Liq} are the total amount of hydrogen contained in the hydrotreated liquid feed and the additives (dimethyl disulfide, aniline), $H^{out}_{Light\ HC}$ is the amount of the hydrogen contained in light hydrocarbons and $H^{out}_{H_2S}$ is the amount of hydrogen contained as H_2S in the gas phase.

2.6 Samples Characterization

2.6.1 Liquid Samples Characterization

Feed and daily liquid products were characterized by a densimeter for determining the density, by chemiluminescence for the nitrogen content, by X-Ray fluorescence spectrometry for the sulfur

content and gas chromatography for the simulated distillation. At the end of the test, the product samples were also analyzed by combustion and thermal conductivity detection to measure the carbon and hydrogen contents and by UV spectrometry to identify the different aromatic families.

In the case of the nitrogen compounds families, feed samples were analyzed by Fourier transform ion cyclotron resonance mass spectrometry (FT-ICR/MS). The analyses were carried out using an LTQ FT Ultra Mass Spectrometer FT-ICR/MS (ThermoFisher Scientific, Bremen Germany) equipped with a 7T magnet (Oxford Instruments), electrospray ionization (ESI) ion source in both polarities (ThermoFisher Scientific, Bremen Germany). With this ionization source, the technique can identify polar heteroelement compounds [53–55]. The ESI+ ionization mode is selective to basic nitrogen compounds, the ESI- mode to neutral nitrogen compounds. Mass range was set to m/z 98-1000. Seventy scans with 4 µ-scans were recorded with an initial resolution set to 200 000. The sample preparation conditions are shown in Table 2.

Table 2. Samples preparation conditions for FTC-IR-MS analysis.

		ESI (+)	ESI (-)
Dilution level	**(%v/v)**	1 Toluene	1 Toluene
Mix of solvents	**(%v/v)**	75/25 (Toluene/Methanol)	75/25 (Toluene/Methanol)
Additive added	**(%v/v)**	1 (Acetic Acid)	1 (Ammonium Hydroxide)

2.6.2 Catalyst Characterization

After catalyst unloading, the spent samples were submitted to an extraction with toluene in a soxhlet extractor at 250°C for 7 h and dried under vacuum at 120°C for 12 h before being submitted to the following analyses. The catalyst surface area, total pore volume, and pore size distribution were measured by nitrogen adsorption-desorption in an ASAP 420 Micromeritics apparatus. The

surface area was calculated from the BET equation, the total pore volume was deduced from the N_2 adsorption at the endpoint of the isotherm and the micropore volume was determined from the t-plot method the Harkins-Jura formula, in the range from 0.35 to 0.50. The uncertainty of surface area and volume measurements is 5% and 2.5%, respectively. The pore size distribution was calculated from the desorption branch of the N_2 isotherm using the BJH model.

The carbon, hydrogen and nitrogen content determination was carried out on a Thermoscientific FlashSmart equipment. Additionally, the catalyst was analyzed by elemental thermogravimetry on a thermobalance Mettler ToledoTGA-DSC1 coupled with mass spectroscopy (Thermostar/Pfeiffer). The MoS_2 sheets were visualized and analyzed by transmission electron microscopy with a JEOL JEM 2100F microscope to determine the slab length and the promoter segregation. The samples were prepared in three steps. In the first step, the catalyst was milled to a fine powder. Then it was dispersed in ethanol in an ultrasonic bath; two drops of the solution were deposited on a copper grid. Finally, the solvent was evaporated, and the sample was introduced into the microscope. The TEM images were recorded in bright field mode. The average dispersion of the MoS_2 particles was calculated from the slab length distribution, assuming a hexagonal shape of the particles [56]. The promoter segregation was investigated by TEM–EDX detection, leading to Ni/Mo ratio calculated for about 25 particles.

2.6.3 Catalytic tests with model molecules

The residual activity of the spent catalysts was assessed for both the hydrogenating and isomerizing/cracking activities. To evaluate the hydrogenating function, the activity was determined by quantifying the hydrogenated products during toluene hydrogenation. The methodology used is described elsewhere [57]. An equivalent protocol was followed regarding the acid function but using the hydroconversion of n-heptane as a model reaction. The catalytic tests were carried out in a fixed bed reactor unit, in the presence of H_2S (generated by decomposition

277 of DMDS) under hydrogen pressure. Catalysts samples were sulfurized in situ at 350°C during 2
278 hours. The operating conditions for each experiment are presented in Table 3.

279 **Table 3. Operating conditions of the catalytic tests with model molecules.**

		Toluene Hydrogenation	n-Heptane Hydroconversion
Concentration of reactant	wt %/feed	20*	95.15
DMDS concentration	wt %/feed	6	4.85
P	MPa	6	6
LHSV	h^{-1}	2	4
T	°C	350	350/360/380
H_2/HC	NL/L	450	330

280 * in cyclohexane as solvent

281

282 # 3 RESULTS

283 ## 3.1 Apparent kinetic constants

284 The evolution of the global net conversion during the long-term tests for both feeds is represented
285 in Figure 5. The performance for the short-term tests was very close to the corresponding period
286 of the long test, so the related data are not shown. As expected, the curves exhibited a lower
287 conversion for feed A, which was heavier and had a higher organic nitrogen content than feed B.
288 The loss of conversion under the accelerated deactivation protocol conditions was more
289 appreciable for feed A than for feed B.

290 One can further observe that the contribution of the first reactor to overall conversion (20% for
291 feed A and 40% for feed B) was lower than that of the second reactor. The distillation curves of
292 the final effluents of the long-term experiment at the first and second reactor outlets are shown in
293 Figure 6. No significant shift with respect to the related feed was observed for the effluents from
294 the first reactor. This behavior was not observed in the case of the effluents from the second
295 reactor. It suggests that cracking reactions in the first reactor were limited; the conversion in the

first reactor was mainly due to dealkylation and hydrogenation reactions carried out on the metal function.

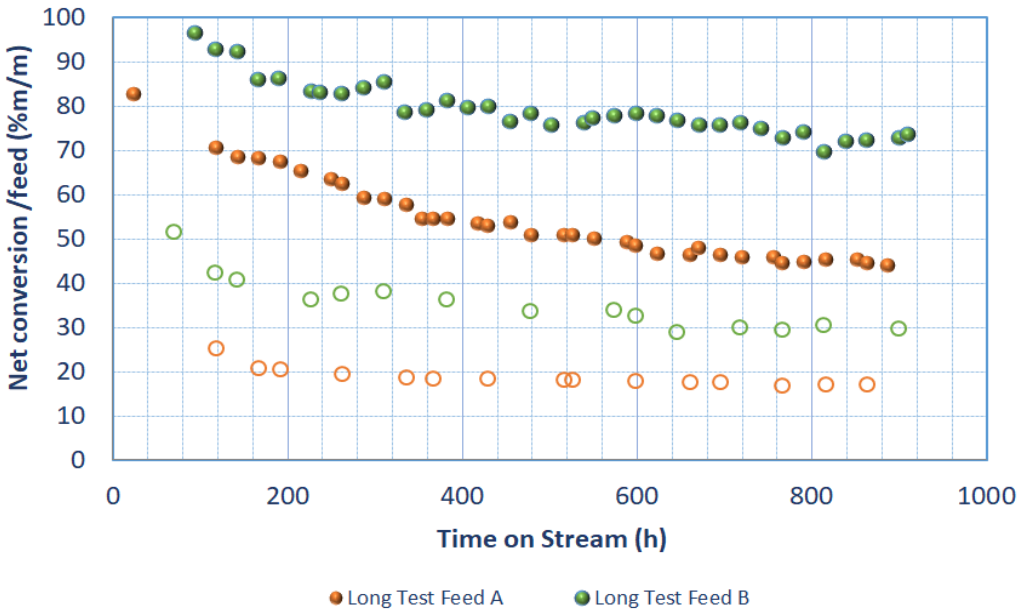

Figure 5. Net conversion evolution with time on stream during long tests with feed A and feed B Full symbols=Total effluent, open symbols=First reactor effluent.

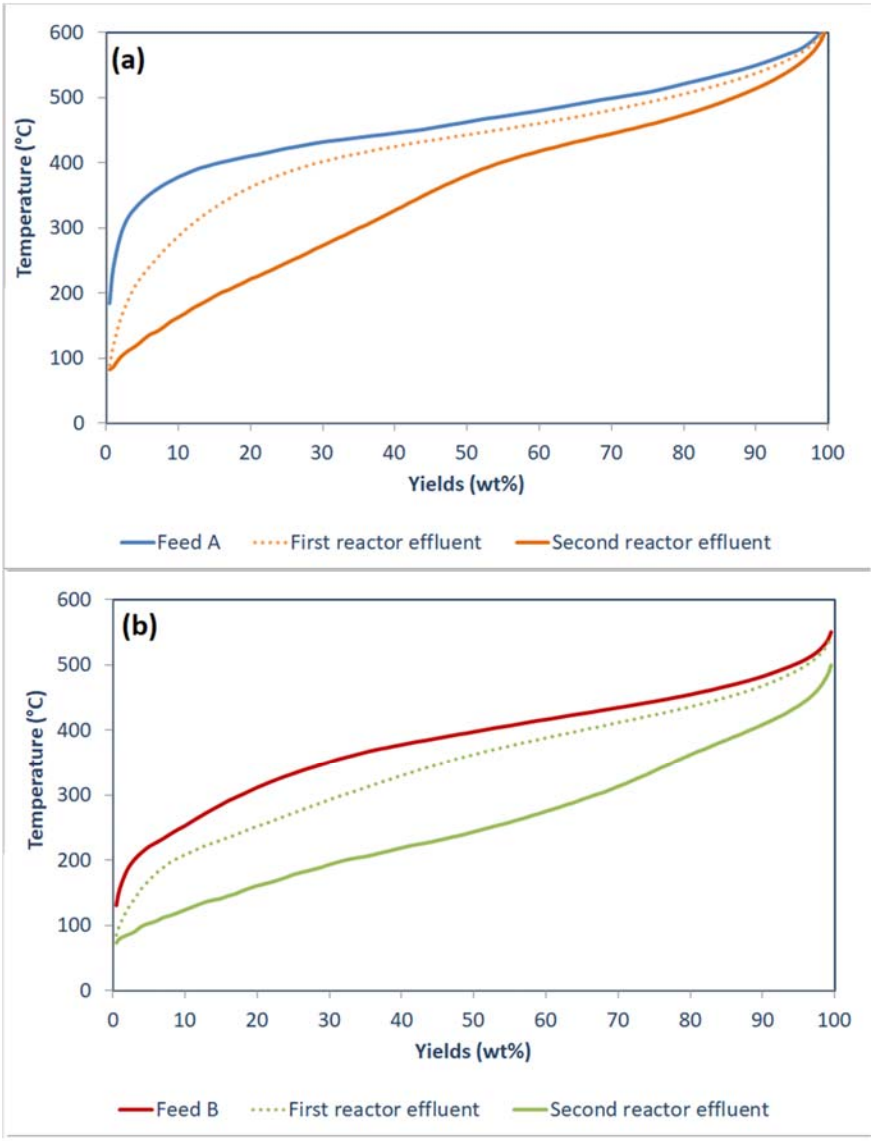

Figure 6. Simulated distillation curves obtained for the feed, first reactor outlet, second reactor outlet with a) feed A, b) feed B for the long-term tests. Dotted line=First reactor effluent, continuous line=Total effluent.

The evolution of the apparent kinetic constants of the relevant chemical reactions (cracking, HDN, HDA and HDS) with time on stream (TOS) is shown in the figures below. Both the global performance of the two reactors and the one for the first reactor are presented for the two different feeds during the long-term test.

Regarding the global performance, the data for the cracking constants (Figure 7) showed that, as was foreseeable, feed B was more reactive than feed A. The rate coefficients of the HDN reactions (Figure 8) were also higher for feed B. This can be attributed to the lower amount of carbazole, benzocarbazole and acridine in this feed (Figure 3), identified among the most refractory compounds in the neutral and the basic nitrogen families [55,58,59]. The higher degree of alkyl substitution (Figure 4) of the nitrogen heterocycles in feed A further reduces their reactivity [43].

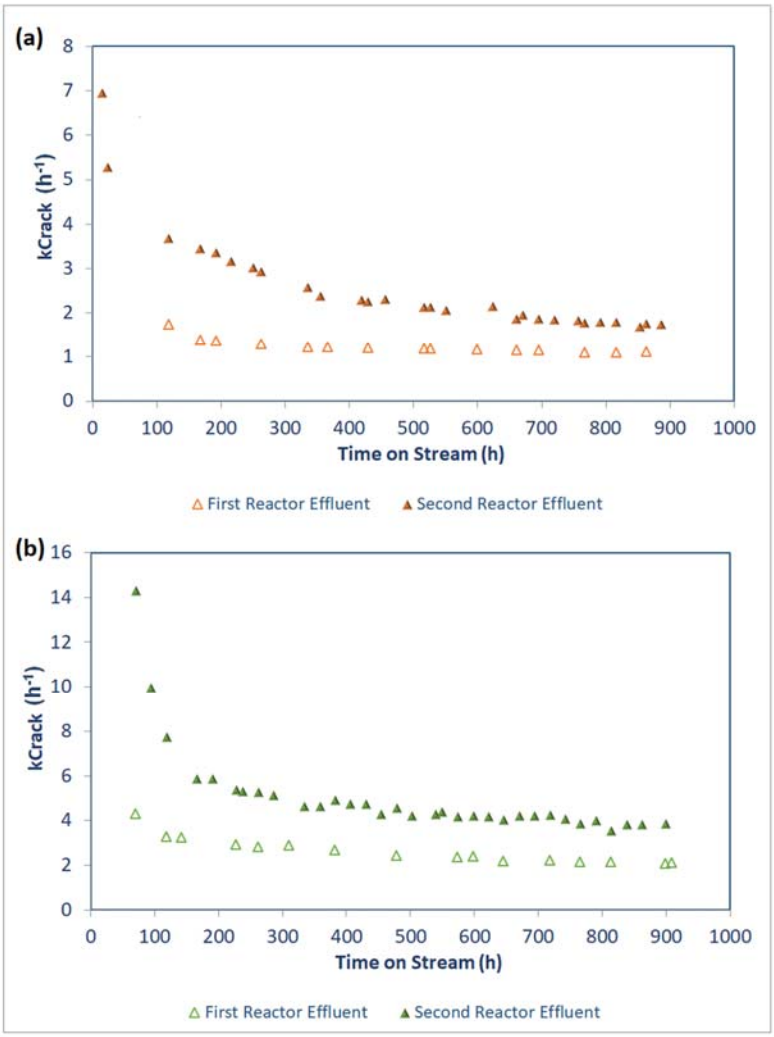

Figure 7. Global and first reactor kinetic constants evolution with time on stream for cracking reactions. a) Feed A and b) feed B. Open symbols=First reactor effluent, Full symbols=Total effluent.

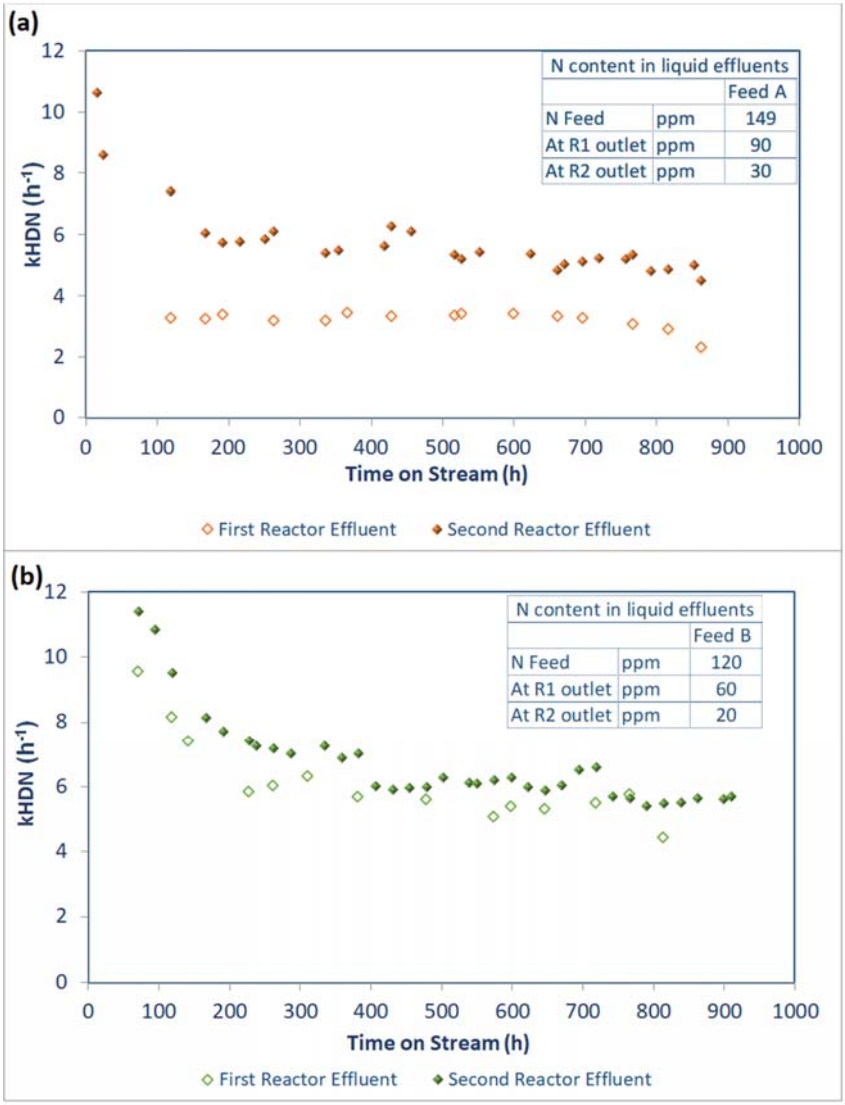

Figure 8. Global and first reactor kinetic constants evolution with time on stream for HDN reactions. a) Feed A and b) feed B. Open symbols=First reactor effluent, Full symbols=Total effluent.

Concerning the HDS kinetic coefficients, those remained nearly constant during the tests and had very similar values for both feeds (not shown). The HDA reaction rate was lower for feed B (Figure 9). It is related to the origin of feed B, which is composed of streams from processes that promote the cracking reactions (LCO from fluid catalytic cracking and HCGO from delayed coking), reducing the alkyl chains, therefore, produce more condensed aromatic structures which have a refractory character to the hydrogenation.

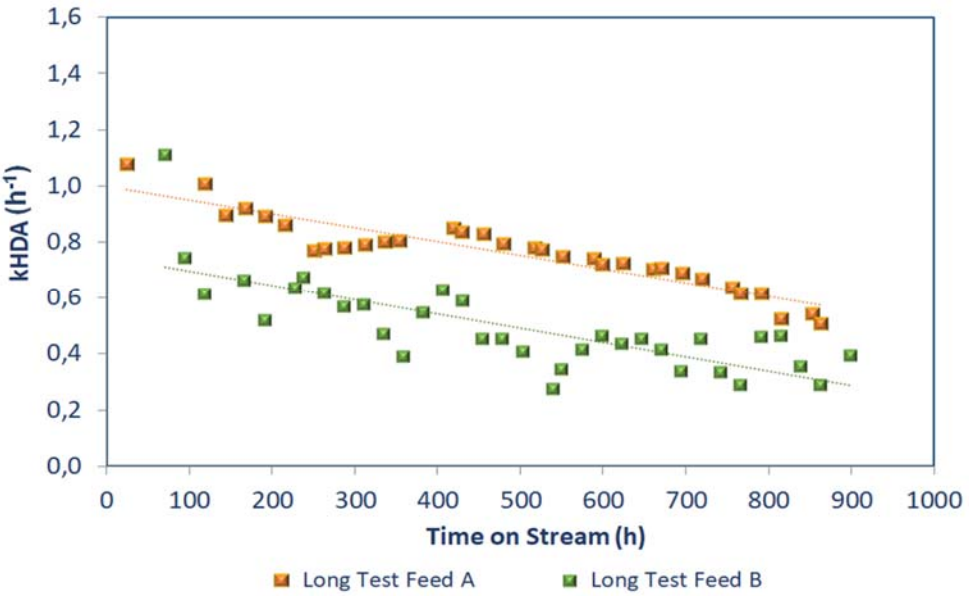

334

335 **Figure 9. Global and first reactor kinetic constants evolution with time on stream for HDA**
336 **reactions.**
337

338 ## 3.2 Quantification of the deactivation rate

339 In the first reactor, all the kinetic constants were lower than in the second reactor. The nitrogen
340 content for both feeds was so high that it provoked a strong inhibition of the hydrotreating reactions
341 and an almost total inhibition of cracking reactions [4]. The cracking reaction rate was nearly stable
342 for the first reactor. The inhibition of the acid function was so strong that no additional deactivation
343 was observed.

344 With time on stream, the catalysts lost activity, the kinetic rates for cracking, HDN and HDA
345 reactions decreased for both feeds. The loss in activity was more significant for cracking and HDN
346 than for HDA reactions. The decrease in the kinetic rates was significantly faster at the beginning
347 than at the end of the test. The loss in cracking activity was also reflected in a decrease of H_2
348 consumption (see supporting information S6).

349 As it was stated, the experimental data for the cracking kinetic constant was fitted with both an
350 exponential and a hyperbolic decay function (Supporting information, **Erreur ! Source du renvoi**

introuvable., **Erreur ! Source du renvoi introuvable.**). Table 4 displays the model parameter values for the activity loss rate, α, for both feeds during the long-term tests. This coefficient accounts for both inhibition and deactivation during the test run.

Table 4. Deactivation coefficients calculated with both an exponential (exp) and a hyperbolic (hyp) decay models.

Case	Time on stream	α_{exp}	α_{hyp}
	days	(1/day)	(1/day)
Feed A	30	0.15	0.18
Feed B	30	0.39	0.57

Feed A was heavier than feed B and had a low reactivity for cracking and HDN reactions; it showed a lower deactivation coefficient than in the case of feed B.

We recall that the inspection of the raw conversion data had suggested the opposite trend: the conversion loss as a function of time was higher for feed A (Figure 5). However, as explained in section 2, it may be misleading to look at raw conversion data. For comprehension purposes, the analysis of the evolution of the apparent rate coefficients is more appropriate.

3.3 Spent catalysts characterization

Samples from the first reactor inlet (Bed In), second reactor inlet (Middle bed) and second reactor outlet (Bed Out) of the catalytic bed were characterized. The samples obtained from the short-term tests (6 days) and long-term tests (30 days) for both feeds were compared.

Results from the elemental analysis are shown in Figure 10 and Figure 11. The catalysts from the tests with feed B had a higher carbon content (Figure 10) with a slightly lower H/C ratio (Figure 11) than the catalysts obtained from the tests with feed A. The carbon content along the reactor increased from the inlet to the outlet for all the samples. Furthermore, the aromatic character (inverse of H/C ratio) of coke deposits also increased in the same sense, in line with the work of Koizumi et al. [27]. This tendency was confirmed by TGA. The coke gradient from bed inlet to bed

outlet can be explained by the inhibition of the coke formation by organic nitrogen, which progressively decreases from bed inlet to bed outlet.

With respect to time evolution, most of the coke was formed at the start of run for both feeds (Figure 10). The H/C ratio (Figure 11) diminished with time because of the dehydrogenation of the carbon deposits initially formed.

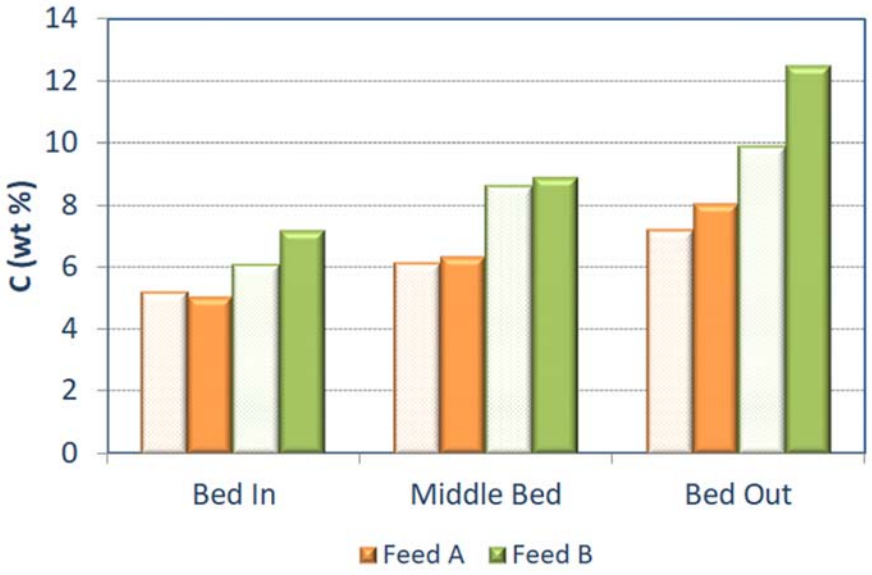

Figure 10. Carbon content of the spent catalysts. Full bars=30 days tests, open bars=6 days tests.

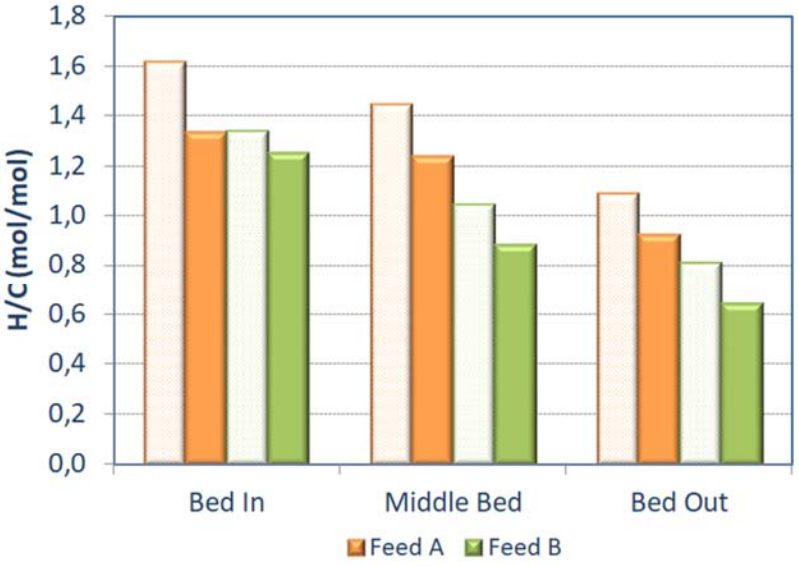

Figure 11. Hydrogen/Carbon (H/C) ratio of the spent catalysts. Full bars=30 days tests, open bars= 6 days tests.

The N/C ratios of the spent catalyst samples are displayed in Figure 12. The values were similar to the ratio of typical organic nitrogen compounds in vacuum gas oils (molecules containing 20 to 40 carbon atoms and one nitrogen atom). The nitrogen proportion in the deposited coke was higher for feed A than for feed B samples. It correlates with the higher nitrogen concentration in feed A. Spent catalyst from the tests with feed B had more deposited coke with a lower N/C ratio than samples from feed A. It means that the contribution of aromatics coke precursors was more significant for feed B, which was related to the higher aromatics content in this feed.

The values of the N/C ratio decreased along the reactor, which agrees with the profile of nitrogen concentration, which shows a maximum at bed inlet. The nitrogen compounds are strongly adsorbed in the acid sites and formed coke because its desorption rate is slow compared to the coke reactions rate. With time on stream, the N/C ratio (Figure 12) decreased.

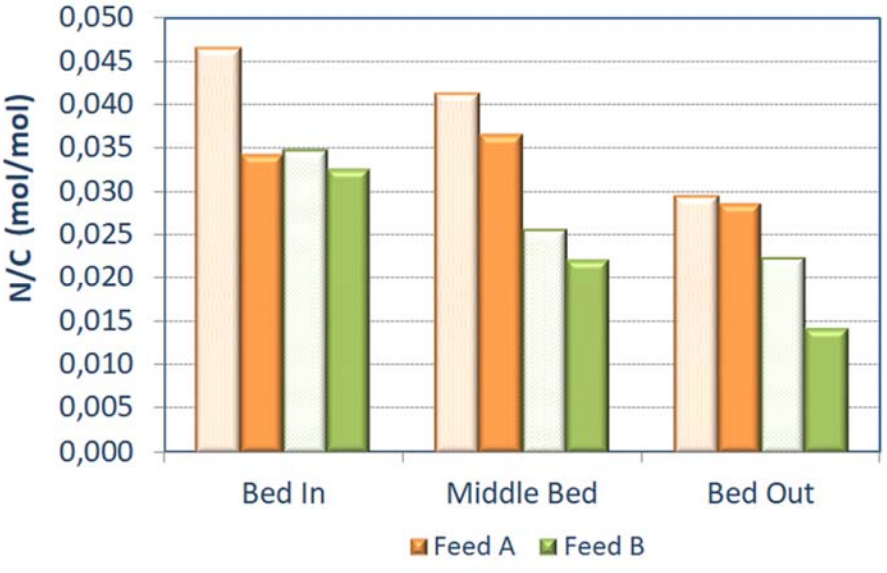

Figure 12. N/C ratio of the spent catalysts. Full bars=30 days tests, open bars= 6 days tests.

The coke deposit influenced the catalyst textural properties since it reduced the available pore volume and the surface area. Table 5 shows the losses in surface area (S) and pore volume (V) for the spent samples compared to the fresh catalyst. The samples from the tests with feed B, with the higher carbon contents, also exhibited the highest losses of surface area and pore volume. In the same sense, for both feeds, the loss in textural properties was more pronounced for the samples obtained from the second reactor, where the carbon deposition was also enhanced. Surface area and pore volume slightly decreased with time on stream (except for the first reactor with feed A because the coke deposition was controlled by the nitrogen inhibition). The losses of surface and pore volume were proportional to the amount of deposited coke (see supporting information **Erreur ! Source du renvoi introuvable.** and **Erreur ! Source du renvoi introuvable.**).

Table 5. Characterization of spent catalysts: Surface area (S), total pore volume (V) and micropore volume (μV) of the spent catalyst relative to the fresh catalyst.

Sample	Time on stream	S/S_{fresh}		V/V_{fresh}		$\mu Vol/\mu Vol_{fresh}$	
		Bed Inlet	Bed Outlet	Bed Inlet	Bed Outlet	Bed Inlet	Bed Outlet
	days	(%)	(%)	(%)	(%)	(%)	(%)
Feed A	6	86	82	80	75	71	71
Feed A	27	86	78	81	71	71	65
Feed B	6	85	75	81	70	67	65
Feed B	27	82	71	78	69	61	65

TEM/EDX analysis was performed on the spent catalysts to evaluate the morphology of the MoS_2 slabs and their Ni/Mo ratio (see supporting information Table S2). As expected, slab length, average dispersion and Ni/Mo ratio in the slabs did not significantly depend on the type of feed used. There were also no remarkable evolutions as a function of time on stream or as a function of the location in the reactor. However, a slight sintering of the MoS_2 slabs and a significant nickel

depromotion have been observed in our previous study [38]; these results mean that sintering and depromotion took place in the initial stages and then the slab morphology reached a steady state.

Catalytic assays evaluated the residual catalytic activity of the spent samples with model molecules, toluene hydrogenation for the (de)hydrogenating function and heptane hydroconversion for the acid function. The fresh catalyst presented a toluene conversion of 70% and a n-heptane conversion of 95%. The obtained results are illustrated in Figure 13. It is clear that there was an activity loss of both functions, compared to fresh catalyst, even more pronounced for the acid function. The solids from the tests with Feed A exhibited a higher residual hydrogenation activity but a lower cracking/isomerization activity than the solids from the tests with feed B.

The deactivation of the metal function increased along the catalytic bed; this behavior was more pronounced with feed B samples. However, this loss of activity did not strongly depend on time on stream. Since the depromotion for all the samples under the deactivation conditions was similar, the observed differences between the solids from the tests with both feeds can be related to the carbon deposition on the catalysts (Figure 15a). For the acid function, the performance was the opposite. The number of available acid sites in the second reactor was higher than in the first one, despite a higher carbon content. This tendency was more marked with feed B. This will be discussed in section 4.

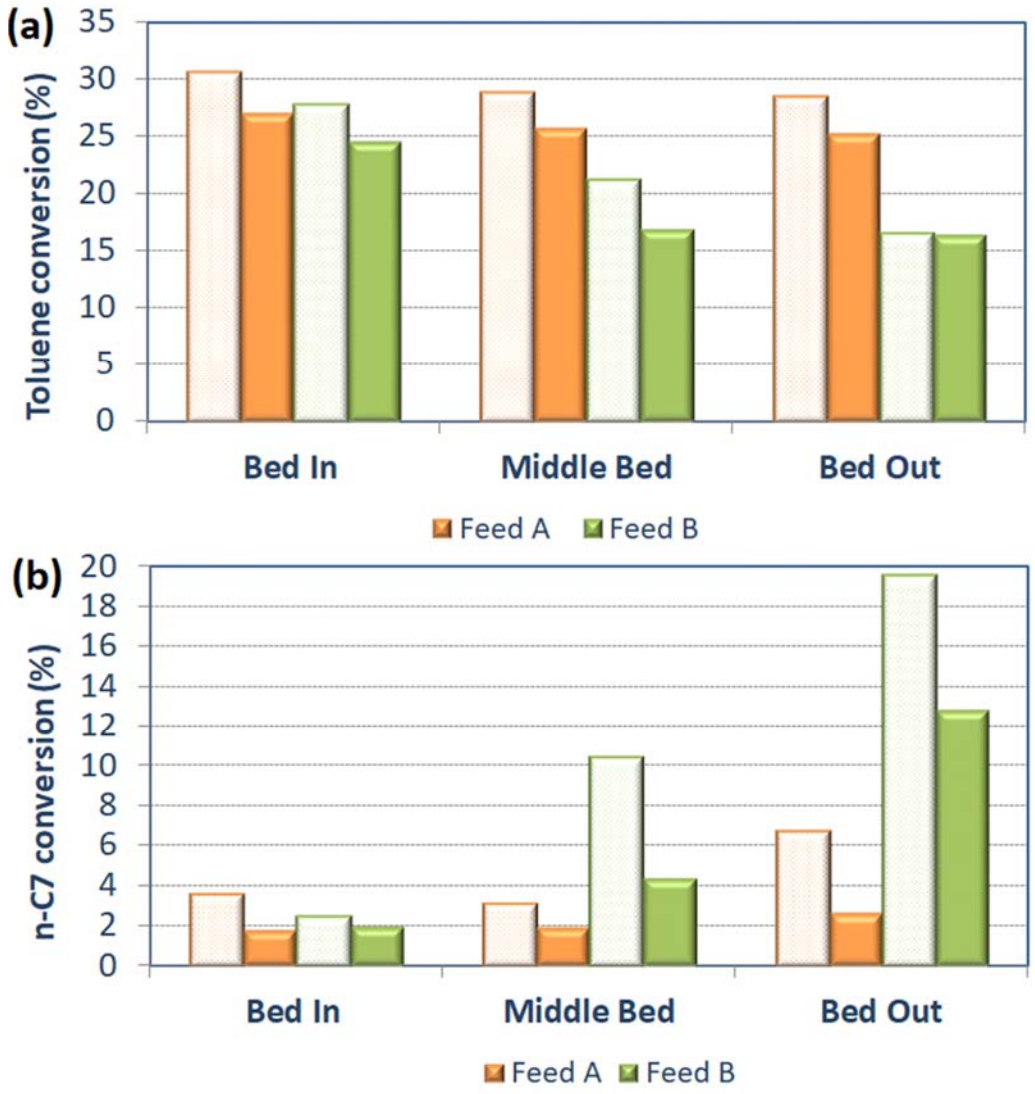

Figure 13. Residual catalytic activity evaluated by model molecules catalytic tests a) Hydrogenation of toluene, b) Isomerization/cracking of n-heptane at 360°C. Full bars=30 days tests, open bars= 6 days tests.

The selectivity towards i-heptane formation (the primary product) in the n-heptane hydroconversion can be considered as an indicator of the metal/acid balance (as compared at the same conversion level) [60,61]. The higher the selectivity, the higher the hydrogenation activity of the metal sites compared to the activity of the acid sites. In contrast, a low i-heptane selectivity means that the acid sites are not well balanced by the hydrogenation sites. Figure 14 represents the selectivity performance for the samples obtained during the processing of both feeds. Spent

samples from tests with feed A showed higher i-heptane selectivity than the ones from feed B. It is in line with the fact that those samples presented the highest hydrogenation activity and the lowest cracking activity. It reinforces the balance of metal/acid sites and, in this way, the selectivity to i-heptane.

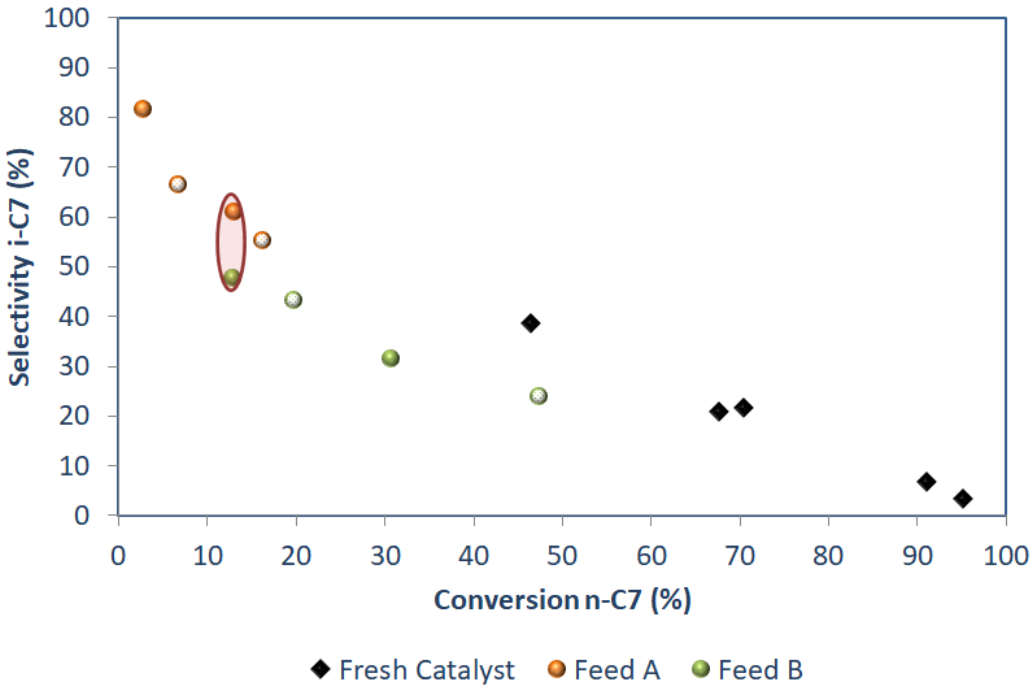

Figure 14. Test n-heptane Selectivity to i-C7 Vs. conversion n-C7 at 350, 360 and 380°C. Open symbols= 6 days tests, full symbols=30 days tests. Bed outlet samples.

4 DISCUSSION

4.1 Evolution with time

During time on stream, the catalysts presented a loss in activity; the kinetic rates for cracking (Figure 7), HDN (Figure 8) and HDA (Figure 9) reactions decreased for both feeds. The deactivation of cracking and HDN activity was very pronounced in the first 150 h, followed by slower, more gradual decay. These results agree with different works [33,62,63] that reported a faster activity decay at the beginning of the run.

471 Regarding the carbon content evolution with time, the data (Figure 10) indicated that the major
472 part of the coke was formed at the beginning of the tests for both feeds. During the first 6 days on-
473 stream after performance stabilization, between 90 and 95% of total final coke was deposited for
474 feed A and between 80 and 85% for feed B. It is consistent with the literature [62,64,65] that
475 claims that coke deposition initially increases rapidly before a pseudo-stable state is reached. For
476 reforming catalysts, Querini [66] et Absi-Halabi [64] found that coke equivalent to 25% of the
477 weight of the original catalyst is deposited within the first few hours of operation. The increase of
478 the coke deposition with time was smaller for feed A than for feed B due to the higher inhibition of
479 the coke reactions by nitrogen compounds. The H/C ratio (Figure 11) also decreased with time
480 because as condensation and polymerization reactions to form coke progress, dehydrogenation
481 occurs [26,27,33,67]. This evolution of the coke deposition correlates with the observed
482 performance for the deactivation rate. As was expected, textural properties followed the same
483 behavior as coke deposition. Thus, there was no meaningful change in the first reactor for feed A
484 with time on stream because the coke deposition was controlled by the nitrogen inhibition, which
485 was more important than in the second reactor.

486 The amount of N which was deposited on the catalyst also did not evolve much any longer after
487 150 h on stream. On the other hand, the N/C ratio (Figure 12) continued to decrease with time, in
488 agreement with previous works [68], which state that as the catalysts ages, N/C ratios decrease.
489 This may be related to the preferential adsorption of the nitrogen compounds on the acid sites
490 [35,64]. These adsorbed compounds in the early stages form coke precursors with moderate
491 aromaticity (relatively high H/C ratio). Subsequent accumulation of coke results from the
492 condensation/polymerization reactions of the unsaturated intermediates formed preferentially from
493 aromatic structures, which provokes a reduction in the N/C and H/C ratio.

494 The model molecule tests (Figure 13) allow evaluating the effect of coke formation on the
495 hydrogenation and cracking functions. The hydrogenation activity of the spent catalysts is rather

well correlated with the amount of deposited coke (Figure 15a). The residual hydrocracking activity, however, is totally anticorrelated with the amount of coke (Figure 15

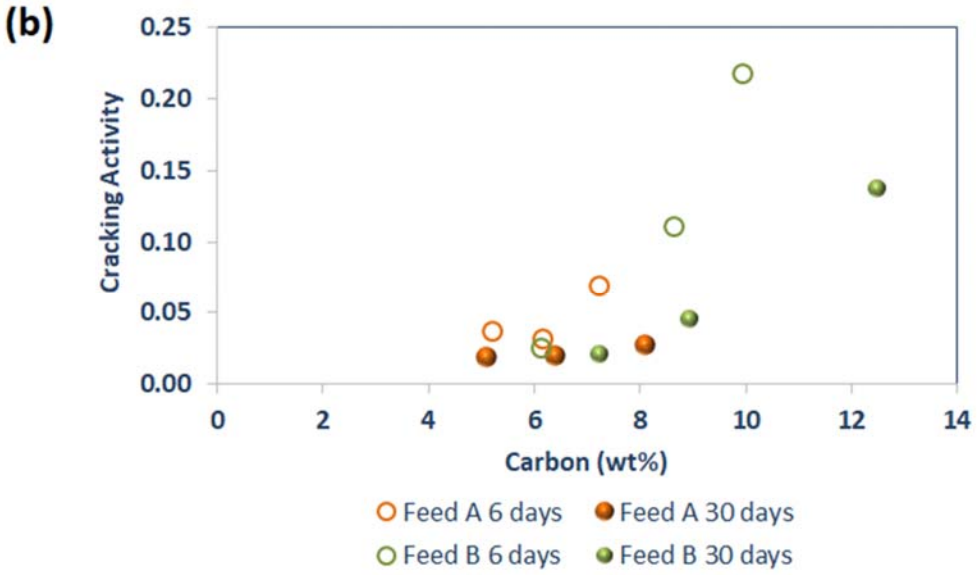

b). It drops drastically in the initial stage and continues to decay gradually (even when the total coke content remains almost constant). The bed outlet always maintains a higher residual cracking activity than the bed inlet, despite the lower carbon content of the latter. The concentration of organic nitrogen compounds in the reactor follows the opposite trend: it decreases from reactor inlet to reactor outlet and increases with time due to the deactivation of HDN. We therefore suppose that the acid sites undergo a very specific deactivation due to nitrogen compounds, which is uncorrelated from the global coke build-up.

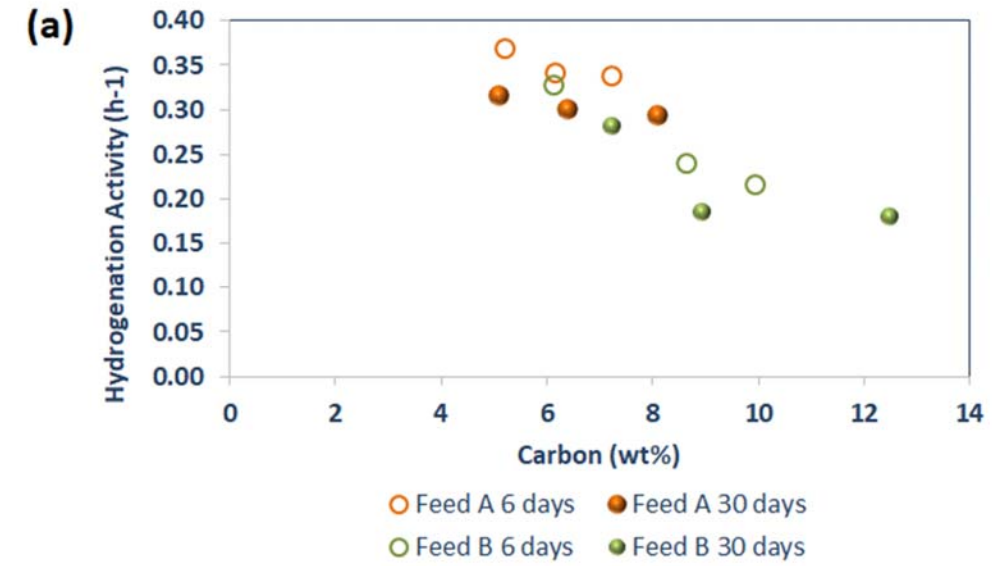

507

508

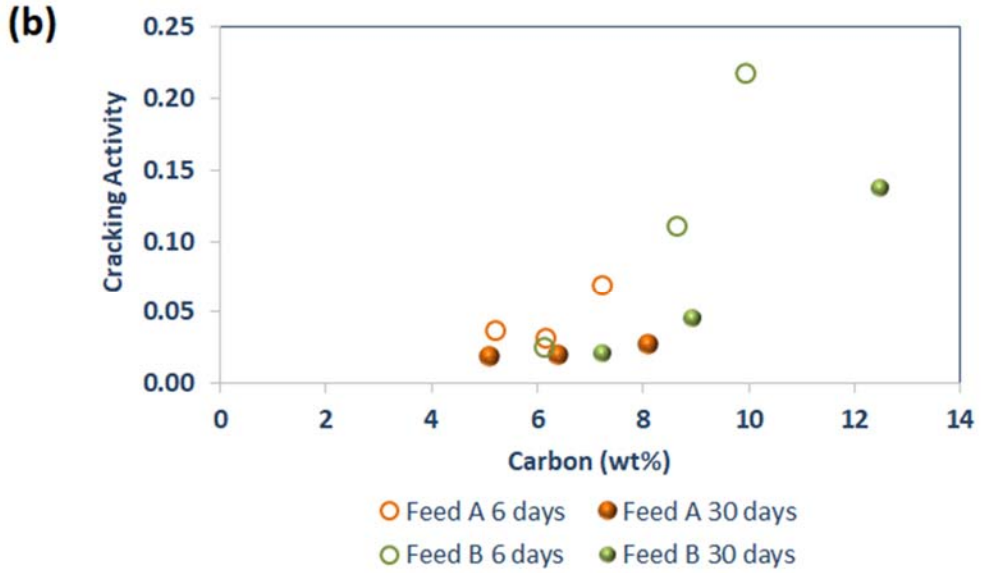

509

510 **Figure 15. Relation between the a) hydrogenation activity and b) n-C7 cracking activity of the**
511 **catalyst and the amount of coke.**

512 ## 4.2 Impact of the feed

513 The effect of the type of feedstock on catalyst deactivation was studied with a hydrotreated VGO,

514 Feed A, and a lighter mixture, Feed B. These feeds had a different organic nitrogen content: 149

515 ppmw for feed A and 120 ppmw for feed B. The nitrogen families in both feedstocks were similar.

However, the distribution of the compounds was different; essentially, feed A contained slightly more acridine (basic nitrogen), carbazoles, benzocarbazoles and dibenzocarbazoles (neutral nitrogen) than feed B. These compounds are the most refractory for the HDN reactions. Additionally, nitrogen compounds of feed A showed higher molecular weight associated with a higher degree of alkyl substitution what decreases the hydrogenation reactivity of these compounds. The aromatics content was ~37 wt% and ~42 wt% for feed A and B, respectively. Monoaromatics were the dominating family within both feeds, followed by diaromatics and triaromatics; the mass fractions of these three families were slightly higher for feed B. This feed is composed of streams from processes that promote the cracking, fluid catalytic cracking (LCO), and delayed coking (HCGO), reducing the alkyl chains, therefore producing more condensed aromatic structures have a refractory character to the hydrogenation.

Both feeds were submitted to the same deactivation conditions during the same time. Results based on the exponential decay function (Table 4) and textural properties of the catalyst (Table 5) showed a lower deactivation rate for feed A. It is consistent with the lower coke deposition on the spent catalysts from the feed A tests (Figure 10). This was unexpected considering the higher molecular weight of feed A and also its higher nitrogen content. The obtained results indicate that these are not the determinant factors of the observed catalyst deactivation. It is rather the nature of the coke precursor molecules, i.e., aromatics and nitrogen compounds. As already mentioned, this nature is dictated by the origin of the feedstocks.

As it was mentioned, feed A had a higher nitrogen concentration and more refractory compounds than feed B. Also, a lower HDN rate was observed during the tests with feed A (Figure 7). Thus, the nitrogen content was higher for feed A than for feed B at the same reactor location. The organic nitrogen compounds are rapidly adsorbed on the acid sites of the catalyst due to their basic character [2,3,37,69]. This adsorption leads first to the inhibition of these sites by neutralization and then to irreversible deactivation by coke deposits since the adsorbed nitrogen compounds

541 react to form coke before being desorbed. Both mechanisms result in the loss of cracking activity
542 [34] and low coke deposition from aromatics [29]. These effects were less significant for feed B
543 because its nitrogen compounds were more reactive and in a lower proportion than feed A. The
544 model molecules tests (Figure 13) pointed out the bigger loss of cracking activity for the catalyst
545 samples obtained from the tests with feed A compared to feed B, except at the first reactor inlet,
546 where the activities were similar and substantially low. However, feed A leads to a lower
547 deactivation rate. As the acid function determines cracking activity, it is concluded that the solids
548 from the tests with feed B had more acid sites available than those from feed A. These sites are
549 poorly balanced by the metal sites as observed in the selectivity results.
550
551 In contrast, the toluene hydrogenation test showed a higher activity loss for all the spent catalysts
552 from the experiments with feed B than with feed A, which was attributed to a higher coke build-up
553 with feed B. As a matter of fact, the TEM/EDX analysis shows no significant differences in terms
554 of MoS_2 slab morphology and Ni/Mo ratio related to the spent catalysts in contact with both feeds.
555 The higher hydrogenating activity for feed A might be related to the higher inhibition of the
556 (de)/hydrogenation reactions by the nitrogen compounds, which also inhibit the coke deposition
557 on the metal surface.
558
559 In summary, spent catalysts from tests with feed A had a higher hydrogenation activity and a lower
560 cracking activity than catalysts from the tests with feed B. Accordingly, the balance between metal
561 sites and acid sites (M/A) of the spent catalysts was different for both feeds. The i-heptane
562 selectivity can assess this balance; results were presented in Figure 14. A high selectivity indicates
563 a high number of active metal sites with respect to acid sites. A low selectivity means that there is
564 an imbalance between the acid sites and hydrogenation sites. Hence the (M/A) ratio was lower in
565 spent catalyst obtained with feed B than with feed A. As a consequence of the different ratio, both
566 quantity and type of deposited coke were also different. Actually, during the test with feed B, since

567 there were more available acid sites, many free radicals and carbocations were formed that
568 undergo polymerization reactions before finding a metal site for being hydrogenated. Therefore
569 there was an increase in the amount of coke with a lower H/C ratio, indicating a more aromatic
570 character from the tests with feed B (Figure 11). So, after all, although feed A leads to a more
571 substantial deactivation of acid sites, this is not the main parameter explaining deactivation. The
572 metal/acid balance explains the extent of coke formation and the ranking of the deactivation rates.

573 The formed coke could originate from the organic nitrogen compounds or other coke precursors
574 like aromatic compounds. To estimate the contribution of each one of them, the N/C ratio values
575 of the spent catalyst were measured (Figure 12). Despite the higher quantity of deposited carbon
576 on the catalysts from the tests with feed B, the values of the N/C ratio were lower. The former
577 suggests that feed B might have an important contribution from aromatic compounds that may
578 condense and form coke deposits reducing the global activity. It is consistent with the higher
579 amount of aromatics.

580 Summing up the higher catalyst deactivation obtained with the lighter feed (feed B) results from
581 two joint facts: more aromatics with low reactivity and a lower nitrogen content with a less basic
582 character and more reactivity, all of this compared to feed A. Herein constituted a strong synergy
583 that leads to a poor balance in the M/A ratio because the fewer nitrogen leads to more available
584 acid sites where the aromatics can form intermediates that undergo condensation/polymerization
585 reactions rather than saturation due to a hydrogenation function also weakened for the low
586 inhibition of the coke formation by nitrogen.

587 # 5 CONCLUSIONS

588 • Combining a feedstock with higher aromatics and a lower nitrogen content creates an
589 imbalance in the ratio M/A, with a low number of metal sites in relation to the acid sites.
590 Consequently, there is poor hydrogenation of the unsaturated coke precursors species

produced in the acid sites, which undergo polymerization and condensation reactions forming the coke deposits on the catalyst surface and promoting its deactivation. This combination has an effect that outweighs the effect of differences in molecular weight and boiling range.

- For a similar type of feed with a similar final boiling point, the total nitrogen and aromatics content significantly impacted the resulting catalyst deactivation. Actually, the key parameters are both the content but mostly the type of nitrogen compounds because they are at the origin of the inhibition of hydrogenation and cracking activities, but even more important, they determine the number of acid sites available for the reactions.

- Independent of the feed properties, the catalyst was strongly deactivated during the first days on-stream. Then, the kinetic rates reached almost constant values. This behavior follows the evolution of coke deposition, which is mainly deposited at the beginning of the test runs. These coke deposits are preferentially formed on the acid sites because of the rapid and strong chemisorption of nitrogen on these sites on one side, and due to condensation and polymerization of aromatics carried out on these sites, on the other side.

- The balance in the metal/acid site ratio determines the amount and type of formed coke. The lower the ratio, the lower the hydrogenation of olefins produced in acid sites, and consequently, the formed coke increases, and its hydrogen content decrease producing a more aromatic (less reactive) coke.

- For the lighter VGO/LCO/HCGO blend cracking, HDS and HDN kinetic constants were higher than for the pure VGO feed. However, the kinetic constant for HDA was lower for the VGO/LCO/HCGO feed. This difference is related to the more condensed aromatic structures of this feed have a refractory character to the hydrogenation because it was composed of

streams from processes (fluid catalytic cracking and delayed coking) that promote side-chain cracking.

Funding sources: This work was supported by IFPEN Energies Nouvelles and ECOPETROL.

Supporting Information:

The supporting information is available free of charge on the ACS publication website: FT-ICR/MS data, ESI (+) and ESI (-) modes focusing on the N1[H] class; exponential decay model; correlation between textural properties and carbon content of spent catalysts; H_2 consumption data; TEM results.

Author Information

Corresponding Author: Gerhard PIRNGRUBER
E-mail: gerhard.pirngruber@ifpen.fr.
ORCID:Gerhard D. Pirngruber: 0000-0003-0688-425X

6 References

[1] Scherzer J, Gruia AJ. Hydrocracking science and technology. New York: Marcel Dekker; 1996.

[2] C.H. Bartholomew. Mechanisms of catalyst deactivation. Applied Catalysis A: General 2001, 2001:17–60.

[3] Vogelaar BM, Eijsbouts S, Bergwerff JA, Heiszwolf JJ. Hydroprocessing catalyst deactivation in commercial practice. Catalysis Today 2010;154(3-4):256–63. https://doi.org/10.1016/j.cattod.2010.03.039.

[4] Furimsky E, Massoth FE. Hydrodenitrogenation of Petroleum. Catalysis Reviews 2005;47(3):297–489. https://doi.org/10.1081/CR-200057492.

[5] Sau M, Basak K, Manna U, Santra M, Verma RP. Effects of organic nitrogen compounds on hydrotreating and hydrocracking reactions. Catalysis Today 2005;109(1-4):112–9. https://doi.org/10.1016/j.cattod.2005.08.007.

[6] Furimsky E (ed.). Catalysts for upgrading heavy petroleum feeds. Amsterdam: Elsevier; 2007.

[7] Voge, H. H., Good, G. M., and B. S. Greensfelder. "Catalytic Cracking of Pure Compounds and Petroleum Fractions.". Third World Petroleum Congress, the Hague: Proceedings 1951, 1951:124.

[8] Wang W, Cai X, Hou H, Dong M, Li Z, Liu F et al. Different Mechanisms of Coke Precursor Formation in Thermal Conversion and Deep Hydroprocessing of Vacuum Residue. Energy Fuels 2016;30(10):8171–6. https://doi.org/10.1021/acs.energyfuels.6b01488.

[9] Voorhies A. Carbon Formation in Catalytic Cracking. Ind. Eng. Chem. 1945;37(4):318–22. https://doi.org/10.1021/ie50424a010.

[10] Furimsky E. Deactivation of hydroprocessing catalysts. Catalysis Today 1999;52(4):381–495. https://doi.org/10.1016/S0920-5861(99)00096-6.

[11] Ancheyta Juárez J. Deactivation of heavy oil hydroprocessing catalysts: Fundamentals and modeling. Hoboken New Jersey: Wiley; 2016.

[12] Dautzenberg, F.M., and de Deken, J.C. Modes of operation in hydrodemetallization. American Chemical Society Dvision of Petroleum Chemistry 1985, 1985.

[13] Richardson SM, Nagaishi H, Gray MR. Initial Coke Deposition on a NiMo/γ-Al2O3 Bitumen Hydroprocessing Catalyst. Ind. Eng. Chem. Res. 1996;35(11):3940–50. https://doi.org/10.1021/ie950761o.

[14] Callejas MA, Martínez MT, Blasco T, Sastre E. Coke characterisation in aged residue hydrotreating catalysts by solid-state 13C-NMR spectroscopy and temperature-programmed

oxidation. Applied Catalysis A: General 2001;218(1-2):181–8. https://doi.org/10.1016/S0926-860X(01)00640-8.

[15] Wiwel P, Zeuthen P, Jacobsen AC. Initial Coking and Deactivation of Hydrotreating Catalysts by Real Feeds. In: Bartholomew CH, Butt JB, editors. Catalyst deactivation, 1991: Proceedings of the 5th international symposium, Evanston IL, June 24-26, 1991. Amsterdam, Oxford, New York: Elsevier; 1991, p. 257–264.

[16] K. Matsushita, R. Koide, S. Fukase, A. Stanislaus, A. Al-Barood, F. Al-Jasem, M. Absi-Halabi. American Chemical Society Dvision of Petroleum Chemistry 2000, 2000.

[17] C.H. Yang, S.F. Chen, H. Chen and F. Du. American Chemical Society Dvision of Petroleum Chemistry 2002, 2002.

[18] Delmon B, Froment GF. Catalyst Deactivation 1987: International Symposium Proceedings. Burlington: Elsevier; 1987.

[19] Pazos JM, Gonzalez JC, Salazar-Guillen AJ. Effect of catalyst properties and operating conditions on hydroprocessing of high-metals feeds. Ind. Eng. Chem. Proc. Des. Dev. 1983;22(4):653–9. https://doi.org/10.1021/i200023a018.

[20] Tamm PW, Harnsberger HF, Bridge AG. Effects of feed metals on catalyst aging in hydroprocessing residuum. Ind. Eng. Chem. Proc. Des. Dev. 1981;20(2):262–73. https://doi.org/10.1021/i200013a014.

[21] Johnson BG, Massoth FE, Bartholdy J. Diffusion and catalytic activity studies on resid-deactivated HDS catalysts. AIChE J. 1986;32(12):1980–7. https://doi.org/10.1002/aic.690321207.

[22] Trimm DL. Catalyst design for reduced coking (review). Applied Catalysis 1983;5(3):263–90. https://doi.org/10.1016/0166-9834(83)80156-0.

[23] Barbier J, Corro G, Zhang Y, Bournville JP, Franck JP. Coke formation on bimetallic platinum/rhenium and platinum/iridium catalysts. Applied Catalysis 1985;16(2):169–77. https://doi.org/10.1016/S0166-9834(00)84470-X.

[24] Barbier J. Deactivation of reforming catalysts by coking - a review. Applied Catalysis 1986;23(2):225–43. https://doi.org/10.1016/S0166-9834(00)81294-4.

[25] Sahoo SK, Ray SS, Singh ID. Structural characterization of coke on spent hydroprocessing catalysts used for processing of vacuum gas oils. Applied Catalysis A: General 2004;278(1):83–91. https://doi.org/10.1016/j.apcata.2004.09.028.

[26] AMEMIYA M, KORAI Y, MOCHIDA I. Catalyst Deactivation in Distillate Hydrotreating (Part 2) Raman Analysis of Carbon Deposited on Hydrotreating Catalyst for Vacuum Gas Oil. J. Jpn. Petrol. Inst. 2003;46(2):99–104. https://doi.org/10.1627/jpi.46.99.

[27] Koizumi N, Urabe Y, Inamura K, Itoh T, Yamada M. Investigation of carbonaceous compounds deposited on NiMo catalyst used for ultra-deep hydrodesulfurization of gas oil by means of temperature-programmed oxidation and Raman spectroscopy. Catalysis Today 2005;106(1-4):211–8. https://doi.org/10.1016/j.cattod.2005.07.172.

[28] Speight JG. The chemistry and technology of petroleum. 3rd ed. New York: Marcel Dekker; 1999.

[29] Muegge BD, Massoth FE. Basic studies of deactivation of hydrotreating catalysts with anthracene. Fuel Processing Technology 1991;29(1-2):19–30. https://doi.org/10.1016/0378-3820(91)90014-4.

[30] Girgis MJ, Gates BC. Reactivities, reaction networks, and kinetics in high-pressure catalytic hydroprocessing. Ind. Eng. Chem. Res. 1991;30(9):2021–58. https://doi.org/10.1021/ie00057a001.

[31] Toulhoat H, Raybaud P (eds.). Catalysis by transition metal sulphides: From molecular theory to industrial application. Paris: Éd. Technip; 2013.

[32] Park YC, Rhee H-K. The role of nickel in pyridine hydrodenitrogenation over NiMo/Al2O3. Korean J. Chem. Eng. 1998;15(4):411–6. https://doi.org/10.1007/BF02697131.

720 [33] Breysse M, Furimsky E, Kasztelan S, Lacroix M, Perot G. Hydrogen activation by transition
721 metal sulfides. Catalysis Reviews 2002;44(4):651–735. https://doi.org/10.1081/CR-
722 120015483.
723 [34] Laredo S GC, los Reyes H J de, Luis Cano D J, Jesús Castillo M J. Inhibition effects of
724 nitrogen compounds on the hydrodesulfurization of dibenzothiophene. Applied Catalysis A:
725 General 2001;207(1-2):103–12. https://doi.org/10.1016/S0926-860X(00)00620-7.
726 [35] Dong D, Jeong S, Massoth FE. Effect of nitrogen compounds on deactivation of hydrotreating
727 catalysts by coke. Catalysis Today 1997;37(3):267–75. https://doi.org/10.1016/S0920-
728 5861(97)00022-9.
729 [36] Kaernbach W, Kisielow W, Warzecha L, Miga K, Klecan R. Influence of petroleum nitrogen
730 compounds on hydrodesulphurization. Fuel 1990;69(2):221–4. https://doi.org/10.1016/0016-
731 2361(90)90178-S.
732 [37] Celis-Cornejo CM, Pérez-Martínez DJ, Orrego-Ruiz JA, Baldovino-Medrano VG.
733 Identification of Refractory Weakly Basic Nitrogen Compounds in a Deeply Hydrotreated
734 Vacuum Gas Oil and Assessment of the Effect of Some Representative Species over the
735 Performance of a Ni–MoS 2 /Y-Zeolite–Alumina Catalyst in Phenanthrene Hydrocracking.
736 Energy Fuels 2018;32(8):8715–26. https://doi.org/10.1021/acs.energyfuels.8b02045.
737 [38] July C. Vivas-Báez, Gerhard Pirngruber, Alberto Servia, Anne-Claire Dubreuil, David J.
738 Pérez-Martínez. Insights in the phenomena involved in deactivation of industrial
739 hydrocracking catalysts through an accelerated deactivation protocol. Fuel 2021, 2021.
740 [39] Dutriez T, Borras J, Courtiade M, Thiébaut D, Dulot H, Bertoncini F et al. Challenge in the
741 speciation of nitrogen-containing compounds in heavy petroleum fractions by high
742 temperature comprehensive two-dimensional gas chromatography. J Chromatogr A
743 2011;1218(21):3190–9. https://doi.org/10.1016/j.chroma.2010.10.056.
744 [40] Stratiev DS, Shishkova IK, Nikolaychuk E, Sharafutdinov IM, Vely A, Mitkova M et al.
745 Relationship of the aromatic structural types in vacuum gas oil to empirical correlations based

746 on bulk properties. Petroleum Science and Technology 2016;34(9):860–5.
747 https://doi.org/10.1080/10916466.2016.1170845.
748 [41] Guillemant J, Berlioz-Barbier A, Albrieux F, Oliveira LP de, Lacoue-Nègre M, Joly J-F et al.
749 Low-Level Fusion of Fourier Transform Ion Cyclotron Resonance Mass Spectrometry Data
750 Sets for the Characterization of Nitrogen and Sulfur Compounds in Vacuum Gas Oils. Anal
751 Chem 2020;92(3):2815–23. https://doi.org/10.1021/acs.analchem.9b05263.
752 [42] Nguyen Minh Tuan. Support acidity effects of NiMo sulfide catalysts in hydrodenitrogenation
753 of quinoline, indole and Coker Gas Oil.: Université de Lyon; 2016.
754 [43] Guillemant J, Albrieux F, Oliveira LP de, Lacoue-Nègre M, Duponchel L, Joly J-F. Insights
755 from Nitrogen Compounds in Gas Oils Highlighted by High-Resolution Fourier Transform
756 Mass Spectrometry. Anal Chem 2019;91(20):12644–52.
757 https://doi.org/10.1021/acs.analchem.9b01702.
758 [44] Ancheyta J, Sánchez S, Rodríguez MA. Kinetic modeling of hydrocracking of heavy oil
759 fractions: A review. Catalysis Today 2005;109(1-4):76–92.
760 https://doi.org/10.1016/j.cattod.2005.08.015.
761 [45] Da Novaes LR, Pacheco ME, Salim VMM, Resende NS de. Accelerated deactivation studies
762 of hydrotreating catalysts in pilot unit. Applied Catalysis A: General 2017;548:114–21.
763 https://doi.org/10.1016/j.apcata.2017.06.040.
764 [46] Ancheyta J, Angeles MJ, Macías MJ, Marroquín G, Morales R. Changes in Apparent Reaction
765 Order and Activation Energy in the Hydrodesulfurization of Real Feedstocks. Energy Fuels
766 2002;16(1):189–93. https://doi.org/10.1021/ef0101917.
767 [47] Ferdous D, Dalai AK, Adjaye J. Hydrodenitrogenation and Hydrodesulfurization of Heavy Gas
768 Oil Using NiMo/Al 2 O 3 Catalyst Containing Boron: Experimental and Kinetic Studies. Ind.
769 Eng. Chem. Res. 2006;45(2):544–52. https://doi.org/10.1021/ie050094r.

770 [48] Pacheco ME, Martins Salim VM, Pinto JC. Accelerated Deactivation of Hydrotreating
771 Catalysts by Coke Deposition. Ind. Eng. Chem. Res. 2011;50(10):5975–81.
772 https://doi.org/10.1021/ie1023595.
773 [49] M. Rashidzadeh A. Ahmad, S. Sadighi. Studying of Catalyst Deactivation in a Commercial
774 Hydrocracking Process (ISOMAX). Journal of Petroleum Science and Technology
775 2011;1(1):46–54.
776 [50] Pachousky RA, Best DA, Wojciechowski BW. Applications of the Time-on-Stream Theory of
777 Catalyst Decay. Ind. Eng. Chem. Proc. Des. Dev. 1973;12(3):254–61.
778 https://doi.org/10.1021/i260047a008.
779 [51] Wojciechowski BW. A theoretical treatment of catalyst decay. Can. J. Chem. Eng.
780 1968;46(1):48–52. https://doi.org/10.1002/cjce.5450460109.
781 [52] Castañeda LC, Muñoz J, Ancheyta J. Comparison of approaches to determine hydrogen
782 consumption during catalytic hydrotreating of oil fractions. Fuel 2011;90(12):3593–601.
783 https://doi.org/10.1016/j.fuel.2010.11.047.
784 [53] Klein GC, Rodgers RP, Marshall AG. Identification of hydrotreatment-resistant heteroatomic
785 species in a crude oil distillation cut by electrospray ionization FT-ICR mass spectrometry.
786 Fuel 2006;85(14-15):2071–80. https://doi.org/10.1016/j.fuel.2006.04.004.
787 [54] Liu M, Zhang L, Zhao S, Zhao D. Transformation of Nitrogen Compounds through
788 Hydrotreatment of Saudi Arabia Atmospheric Residue and Supercritical Fluid Extraction
789 Subfractions. Energy Fuels 2016;30(1):740–7.
790 https://doi.org/10.1021/acs.energyfuels.5b02158.
791 [55] Le Maître J, Paupy B, Hubert-Roux M, Marceau S, Rüger C, Afonso C et al. Structural
792 Analysis of Neutral Nitrogen Compounds Refractory to the Hydrodenitrogenation Process of
793 Heavy Oil Fractions by High-Resolution Tandem Mass Spectrometry and Ion Mobility–Mass
794 Spectrometry. Energy Fuels 2020;34(8):9328–38.
795 https://doi.org/10.1021/acs.energyfuels.0c01160.

[56] Lauritsen JV, Bollinger MV, Lægsgaard E, Jacobsen KW, Nørskov JK, Clausen BS et al. Atomic-scale insight into structure and morphology changes of MoS2 nanoclusters in hydrotreating catalysts. Journal of Catalysis 2004;221(2):510–22. https://doi.org/10.1016/j.jcat.2003.09.015.

[57] Arancon R, Saab M, Morvan A, Bonduelle-Skrzypczak A, Taleb A-L, Gay A-S et al. Combined Experimental and Theoretical Molecular Approach of the Catalytically Active Hydrotreating MoS 2 Phases Promoted by 3d Transition Metals. J. Phys. Chem. C 2019;123(40):24659–69. https://doi.org/10.1021/acs.jpcc.9b08437.

[58] Nguyen M-T, Pirngruber GD, Chainet F, Albrieux F, Tayakout-Fayolle M, Geantet C. Molecular-Level Insights into Coker/Straight-Run Gas Oil Hydrodenitrogenation by Fourier Transform Ion Cyclotron Resonance Mass Spectrometry. Energy Fuels 2019;33(4):3034–46. https://doi.org/10.1021/acs.energyfuels.8b04432.

[59] Shin S, Sakanishi K, MOCHIDA I, Grudoski DA, Shinn JH. Identification and Reactivity of Nitrogen Molecular Species in Gas Oils. Energy Fuels 2000;14(3):539–44. https://doi.org/10.1021/ef990136m.

[60] Giannetto GE, Perot GR, Guisnet MR. Hydroisomerization and hydrocracking of n-alkanes. 1. Ideal hydroisomerization PtHY catalysts. Ind. Eng. Chem. Prod. Res. Dev. 1986;25(3):481–90. https://doi.org/10.1021/i300023a021.

[61] Pirngruber GD, Maury S, Daudin A, Alspektor PY, Bouchy C, Guillon E. Balance between (De)hydrogenation and Acid Sites: Comparison between Sulfide-Based and Pt-Based Bifunctional Hydrocracking Catalysts. Ind. Eng. Chem. Res. 2020;59(28):12686–95. https://doi.org/10.1021/acs.iecr.0c01680.

[62] Moulijn J, van Diepen A, Kapteijn F. Catalyst deactivation: is it predictable? Applied Catalysis A: General 2001;212(1-2):3–16. https://doi.org/10.1016/S0926-860X(00)00842-5.

[63] Froment GF. Kinetic Modeling of Hydrocarbon Processing and the Effect of Catalyst Deactivation by Coke Formation. Catalysis Reviews 2008;50(1):1–18. https://doi.org/10.1080/01614940701803960.

[64] Absi-Halabi M SA. Coke formation on Ctz during hydroprocessing. Applied Catalysis 1991;72:193–215.

[65] Hauser A, Stanislaus A, Marafi A, Al-Adwani A. Initial coke deposition on hydrotreating catalysts. Part II. Structure elucidation of initial coke on hydrodematallation catalysts. Fuel 2005;84(2-3):259–69. https://doi.org/10.1016/j.fuel.2004.08.010.

[66] C.A. Querini, N.S. Figoli and J.M. Parera. Hydrocarbons reforming on Pt-Re-/Al,O,-Cl coked in a commercial reactor. Applied Catalysis 1989, 1989:249–62.

[67] Myers, T.E., Lee, F.S., Myers, B.L., Fleisch, T.H., Zajac, G.W. Resid catalyst deactivation in expanded-bed service. AIChE Symposium Series 1989, 1989:21–31.

[68] Zeuthen P, Cooper BH, Clark FT, Arters D. Characterization and Deactivation Studies of Spent Resid Catalyst from Ebullating Bed Service. Ind. Eng. Chem. Res. 1995;34(3):755–62. https://doi.org/10.1021/ie00042a007.

[69] Khalil I, Celis-Cornejo CM, Thomas K, Bazin P, Travert A, Pérez-Martínez DJ et al. In Situ IR-ATR Study of the Interaction of Nitrogen Heteroaromatic Compounds with HY Zeolites: Experimental and Theoretical Approaches. ChemCatChem 2020;12(4):1095–108. https://doi.org/10.1002/cctc.201901560.

840 **FOR TABLE OF CONTENTS ONLY**

841

842